Scripta Materialia 146 (2018) 260–266

Contents lists available at ScienceDirect

Scripta Materialia

journal homepage: www.elsevier.com/locate/scriptamat

Viewpoint article

The scientific questions and technological opportunities of flash sintering: From a case study of ZnO to other ceramics

Jian Luo

Department of NanoEngineering, Program of Materials Science and Engineering, University of California, San Diego, La Jolla, CA 92093, USA

ARTICLE INFO

Article history:
Received 8 November 2017
Received in revised form 3 December 2017
Accepted 3 December 2017
Available online xxxx

Keywords:
Sintering
Flash sintering
Water-assisted flash sintering
Two-step flash sintering
Field-assisted sintering

ABSTRACT

This viewpoint article critically assesses several scientific and technological questions regarding flash sintering: (1) How does a flash start? (2) What are the possible mechanisms of rapid densifications? (3) What are the electric field/current/potential effects? (4) Can we drastically reduce the flash temperature (or even start a flash at room temperature)? (5) Can we control the microstructures (*e.g.*, fabricate dense nanocrystalline ceramics) by manipulating the electric field/current profile? ZnO is discussed as an examplar but other materials are also critically reviewed. New results of both ZnO and Y_2O_3-statabilized ZrO_2 are presented. Open scientific questions and new technological opportunities are discussed.

1. Introduction

In 2010, Professor Raj and colleagues invented an exciting new sintering technology called "flash sintering" [1,2]. Subsequently, flash sintering was demonstrated for pure and Y_2O_3-stabilized ZrO_2 [1–6], TiO_2 [7,8], ZnO [9–14], $CaCu_3Ti_4O_{12}$ dielectrics [15], spinels [16–18], perovskites [19–22], and many other ceramics [23–31] and composites [32–36]; please also see two recent reviews [37,38].

Fig. 1 illustrates an example of flash sintering of ZnO in air, where an applied DC electric field of 300 V/cm initiates a flash at <600 °C to densify a specimen in ~30 s. The flash leads to an abrupt increase of the electric current that would destroy the specimen without a constraint; with a pre-set maximum current limit, the control system switches (from a constant-voltage mode) to a constant-current mode shortly after the flash. The final specimen density is largely determined by the pre-set maximum current (density) that determines the specimen temperature at the steady state (Fig. 1).

Flash sintering differs from the conventional field-assisted sintering technology (FAST) or spark plasma sintering (SPS) in that the applied electric field is typically higher, the sintering time is shorter, and the environment (furnace) temperature is lower (than the die temperature in SPS), as well as the electric current flows directly through the specimen (*vs.* mostly through the die in normal FAST/SPS). Thus, flash sintering can be cost-effective and energy-efficient. The mechanisms for flash sintering, as well as what are the electric field/current effects on sintering and microstructural evolution, are under scrutiny.

2. Flash Initiation

A mechanism for flash initiation must explain the simultaneous and discontinuous increases in mass transport kinetics and electrical conductivity. The first report of flash sintering proposed three possible mechanisms: (1) Joule heating at grain boundaries that enhances grain boundary diffusion and electrical conductivity; (2) an avalanche nucleation of Frenkel pairs driven by the applied field; and/or (3) a non-linear interaction between intrinsic fields (space charges) and the applied field that produces "a catastrophic change in self-diffusion at grain boundaries" [1]. In more recent reports, Professor Raj and colleagues suggested that flash sintering is associated with "a defect catastrophe that includes unusual generation of electrons, holes and point defects" [39], it can sometimes exhibit an nucleation (incubation) period [40,41], and it produces electroluminescence [22,39,42]. Interestingly, the onset of flash sintering starts in a narrow power density range of 10–50 mW/mm^3 for a broad range of materials [43], a phenomenon that is not yet fully understood.

On the other hand, several groups independently proposed and demonstrated that the flash in numerous material systems starts as a thermal runaway [8,44,45]. One model [8,9,11] that uses a graphical construction method to find the coupled thermal and electric runaway condition is briefly discussed below. Here, the energy conservation law (*i.e.*, a balance between the heat generation and dissipation rates) determines the rise of specimen temperature:

$$\sigma(T_S)E^2V_S = \dot{Q}(T_S, T_F) \quad (1)$$

where E is the electric field, V_S is the volume of the specimen, T_S and T_F

E-mail address: jluo@alum.mit.edu.

https://doi.org/10.1016/j.scriptamat.2017.12.006
1359-6462/

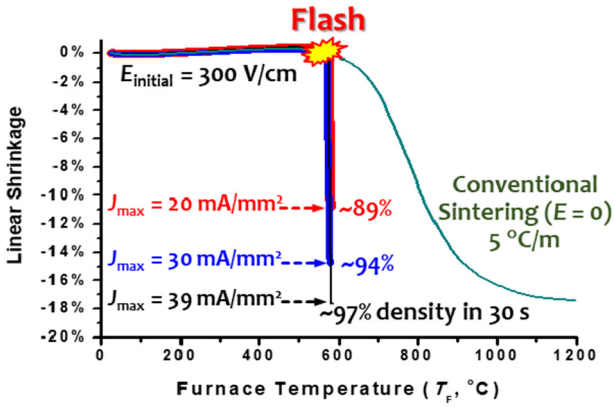

Fig. 1. Examples of the measured linear shrinkage *vs.* furnace temperature curves for flash and conventional sintering of ZnO in air with a constant furnace ramp rate of 5 °C/min. With an initial applied electric field of 300 V/cm, flashes started slightly below 600 °C. The densifications occurred mostly within 30 s. The sintered densities depend on the pre-set maximum current (density) limits. Figure replotted after ref. [11] with revisions.

are the specimen (S) and furnace (F) temperatures, respectively, $\sigma(T_S)$ is the specimen conductivity, and $\dot{Q}(T_S, T_F)$ is the rate of heat dissipation from the specimen. A coupled thermal and electric runaway will occur if there is more heat generated with increasing temperature than that can be dissipated, or:

$$E^2 V_S \left.\frac{d\sigma}{dT}\right|_{T_S} > \frac{\partial \dot{Q}(T_S, T_F)}{\partial T_S} \tag{2}$$

If the blackbody radiation dominates the heat dissipation [$\dot{Q}(T_S, T_F) = A_S \varepsilon \alpha_{Stefan}(T_S^4 - T_F^4)$, where A_S is the surface area of the specimen, ε is the material emissivity, σ_{Stefan} is the Stefan-Boltzmann constant], Eq. (2) can be rewritten as:

$$E^2 \left.\frac{d\sigma}{dT}\right|_{T_S} \frac{V_S}{A_S} > 4\varepsilon\alpha_{Stefan} T_S^3 \tag{3}$$

Eq. (3) suggests a graphical construction method to find the thermal runaway conditions (*e.g.*, Figs. 2 and 3) and the predictions agree well with the observed onset flash temperatures for >10 cases with different materials, doping, particle sizes, and atmospheres [8,9,11,13], attesting the underlying hypothesis that the flash starts as a coupled thermal and electric runaway in these systems. Todd et al. [44] and Dong and Chen [45,46] also proposed and applied similar thermal runaway models on other ceramics.

Figs. 2 and 3 display several additional examples (including six new cases not published before), where the temperature-dependent conductivities $\sigma(T_S)$ were measured from green specimens and extrapolated to predict the thermal runaway conditions that agree with observed flash temperatures within ~5 °C. On one hand, Fig. 2 shows an interesting particle-size dependence of specimen conductivities and the corresponding flash temperatures of ZnO, which can be attributed to the enhanced electronic conduction in the surface layers (with ~10^{12} excess electrons per cm^2 in ZnO [47]) that decreases the flash temperature with the increasing surface area. On the other hand, the surfaces and grain boundaries of 8 mol% Y_2O_3-stabilized ZrO_2 (8YSZ) are insulating so that the powder specimen has lower conductivities that result in a higher flash temperature (Fig. 3); in addition, a reduced atmosphere also decreases the conductivities and subsequently the flash temperature of 8YSZ. Interestingly, both the surface and atmosphere effects in 8YSZ are opposite to those observed in ZnO [9,13], but they can be well explained given the different materials properties of 8YSZ *vs.* ZnO.

Numerous prior reports since 2015 [8,9,11,13,44–46,48,49] and two sets of new systematic results (validations) shown in Figs. 2 and 3

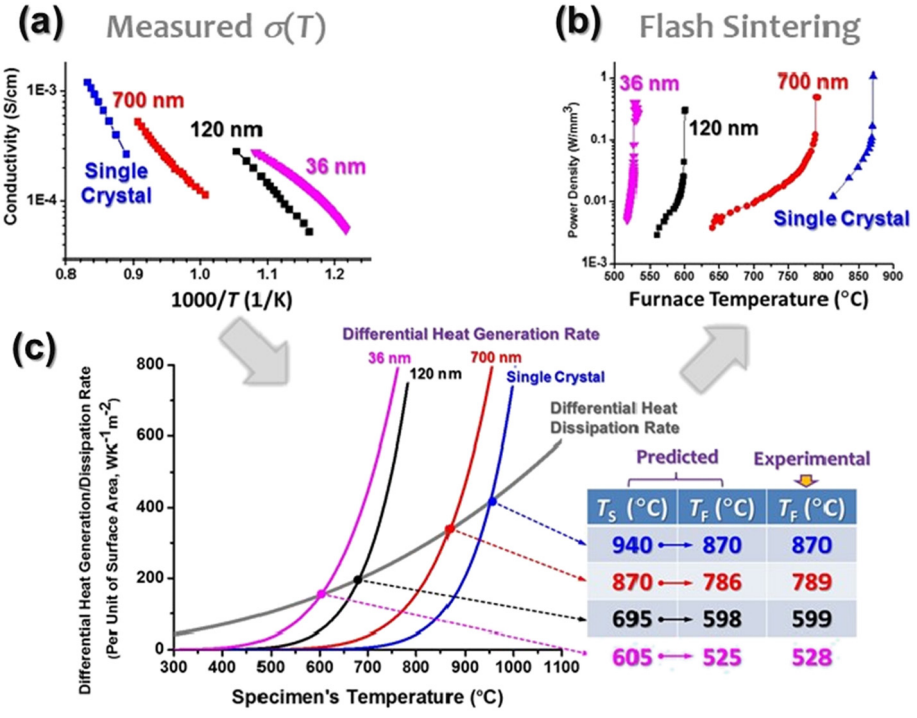

Fig. 2. Flash sintering experiments of three ZnO powder specimens of different particle sizes and a ZnO single crystal in air. (**a**) Measured conductivity *vs.* reciprocal temperature curves of the specimens before the flash sintering. (**b**) Measured power dissipation density *vs.* furnace temperature (T_F) curves during the flash sintering experiments. (**c**) Computed differential heat generation and dissipation rates (per unit specimen surface area) *vs.* specimen temperature curves. In each of the four cases, the thermal runaway condition (the corresponding specimen temperature T_S) can be determined by the intersection of the heat generation and dissipation rates curves; this can then be used to estimate the corresponding furnace temperature (T_F) (using the blackbody radiation model) to compare with observed flash (furnace) temperature shown in panel (b). The single crystal data were taken from ref. [9] and the experimental results of the three powder specimens of different particle sizes are new results originally reported in this viewpoint article.

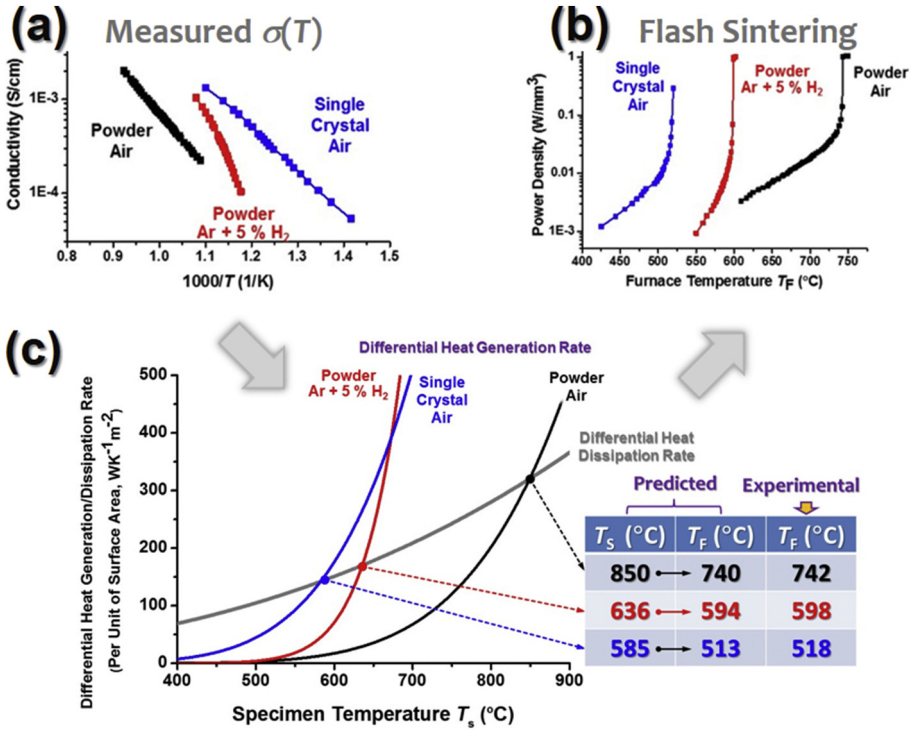

Fig. 3. Flash sintering experiments of three 8 mol% Y_2O_3 stabilized ZrO_2 (8YSZ) experiments, including a single crystal 8YSZ in air and two powder 8YSZ specimens sintered in air and Ar + 5% H_2, respectively. (**a**) Measured conductivity *vs.* reciprocal temperature curves of the specimens before the flash sintering. (**b**) Measured power dissipation density *vs.* furnace temperature curves during the flash sintering experiments. (**c**) In all three cases, the thermal runaway conditions determined by the intersections of the corresponding heat generation and dissipation rates curves agree well with experimentally observed flash temperatures. All data shown in this figure on 8YSZ are new results originally reported in this viewpoint article.

collectively suggest that the flash generally starts as a coupled thermal and electric runaway at least in many, if not all, materials.

Yet, we should recognize the possibilities that in certain materials systems, the occurrence of another physical phenomenon (*e.g.*, a first-order bulk or interfacial transition or avalanche of non-equilibrium defects) with a sudden increase in specimen conductivity can also trigger flash sintering; here, the thermal runaway can be a secondary physical phenomenon (but not the primary cause) that induces the flash. Such mechanisms have not yet been clearly demonstrated. Further research is needed.

3. Possible Rapid Densification Mechanisms

The observed fast densification in flash sintering cannot be explained by simple Arrhenius extrapolations of sintering rates to the estimated specimen temperatures [2,26,50,51]. Thus, the rapid sintering was attributed to a combination of Joule heating and non-equilibrium defect generation, *e.g.*, the "unusual" avalanches of Frenkel defects [2,26,50,51]. However, local electric fields are much lower than that are normally needed for generating Frenkel defects.

To understand the fast densification mechanism of ZnO, a critical comparative study [11] was conducted. This study showed that the flash sintering and benchmarking rapid thermal annealing (RTA, with intensive radiative IR heating) experiments conducted with similar $T(t)$ profiles (with ultrahigh heating rates of ~200 °C/s, followed by isothermal annealing for ~30 s) achieved comparable densification and grain growth rates. This result suggested that the heating profile $T(t)$ (instead of the electric field/current) is the controlling factor for fast densification, at least for pure ZnO. Fig. 4(a) shows the flash sintering and RTA with similar $T(t)$ profiles produces essential identical grain size *vs.* relative density curves, suggesting similar underlying mechanisms. Detailed comparisons of the densification and grain growth rates in the flash sintering *vs.* RTA, which are similar one another with the comparable ~200 °C/s heating rates, can be found in ref. [11].

Furthermore, Todd and co-workers conducted an "ultra-fast firing" experiment for 3YSZ and reached a similar conclusion: "*the accelerated sintering is a consequence of the rapid heating rate involved rather than a direct effect of the electric field on mass transport*" [6]. Their results showed that ultrahigh heat rates can increase the densification rates by >100 times without an electric field [6].

These two studies [6,11] collectively suggest that the ultrahigh heating rate (dT/dt) is a critical factor that lead to fast densification by (1) preventing initial coarsening to keep a high densification driving force and (2) possibly providing non-equilibrium effects. First, sintering is a competition between "densification" and "coarsening"; the latter is relatively faster at lower temperatures and reduces the sintering rate by a factor of $\sim D^4$, where D is the particle/grain size. Thus, an ultrahigh heating rate (dT/dt) to "bypass" the low-temperature coarsening can make a significant difference in the sintering rate (*e.g.*, as small as 10% reduction in coarsening can increase the sintering rate by >50%) [6]. Second, ultrahigh heating rates may also lead to the formation of non-equilibrium grain boundary structures (or "complexions" [52–55]) with enhanced mass transport rates (in comparison with the more relaxed or near-equilibrium grain boundaries) to increase sintering rates [6,56]. Further studies are needed to verify these hypothesized mechanisms.

4. Electric Field/Current/Potential Effects

We should also recognize the possible electric field/current effects on changing the densification rates, which can be pronouncing in certain materials. In a series of elegant studies, Chen and co-workers demonstrated low-temperature electro-sintering of 8YSZ (with large current densities) *via* ionomigration of pores resulted from surface diffusion of Zr cations balanced by the lattice/GB diffusion of oxygen anions [57–59]. This represents an unequivocal demonstration of a significant electric current effect on enhancing the sintering rates with

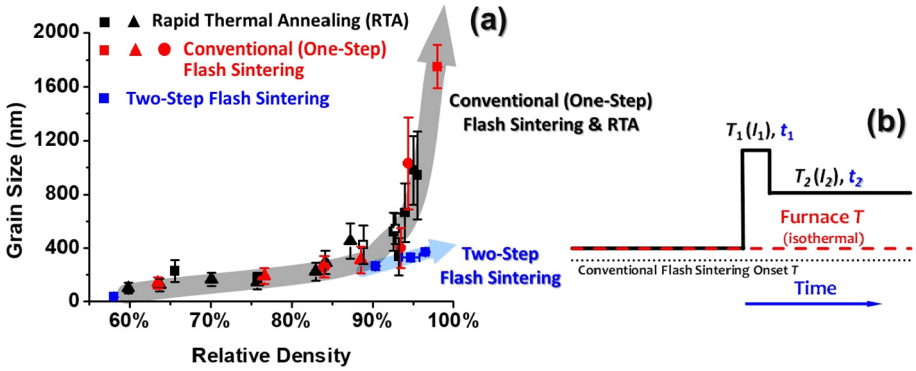

Fig. 4. (**a**) Measured grain sizes *vs.* relative densities for conventional (one-step) flash sintering, rapid thermal annealing (RTA) of comparable $T(t)$ profiles, and two-step flash sintering (TSFS). (**b**) Schematics of two-step flash sintering or TSFS that can enable fast densification with suppressed grain growth. This figure is replotted after combining the data reported in refs. [11,12].

a convincing explanation, although it is not under flash-sintering conditions.

Several more exotic electric field/current effects were recently observed under conditions similar to flash sintering, including: (1) an "anomalous lattice expansion" in 8YSZ [60], (2) reversible emerging and distinguishing of cubic-like phase in 3YSZ during "on-off experiments" at a specimen temperature that the cubic phase should not form [61], (3) accelerated reaction/phase transformation in TiO_2-Al_2O_3 [62], and (4) an apparent "texture change" in TiO_2 (explained as field-induced atomic re-arrangements) [63]. Electric field-induced softening of alkali silicate glasses [64] and phase transformations in (Pb, La)(Zr, Sn, Ti)O_3 single crystals [65] have also been reported.

It is worth noting that earlier studies have already made interesting and intriguing observations of the field effects on grain growth [2]. A relatively weak applied DC or AC field appears to inhibit grain growth of 3YSZ (and subsequently enhance sintering due to smaller grain sizes) [66–71]. Two possible mechanisms have been proposed: (1) the reduction in the grain boundary energy through interactions of the applied fields with the space charges [68,69] or Joule heating at grain boundaries that reduces the grain boundary energy entropically and creates a pinning effect [71].

More recently, Chen and colleagues demonstrated that an applied electric current (of ~50 A/cm^2) could enhance the grain growth in the cathode side discontinuously in 8YSZ [72]. Further studies showed either electrical or hydrogen reduction can depress the local oxygen potential to increase cation kinetics and subsequently enhance grain growth by up to 1000 times in doped zirconia and ceria [72–74]. Cathode-side enhanced grain growth has also been observed in flash-sintered 3YSZ [75].

In general, asymmetrical grain growth, which are likely resulted from electric potential (instead of field or current) effects, has been observed in flash-sintered ZrO_2 [76], 3YSZ [75], $MgAl_2O_4$ [18], UO_2 [77], and ZnO [9], as well as dense 8YSZ [72] and $SrTiO_3$ [78] under electric loadings.

Interestingly, discontinuous (abnormal) grain growth and/or coarsening in the anode side during the flash sintering was observed in ZnO (Fig. 5(a)) [9], which contrasts the cathode-side enhanced grain growth observed in 3YSZ [75] and 8YSZ [72]. This phenomenon can be explained from the possible occurrence of an electric-potential-induced grain boundary oxidation transition *via* combining Tuller's theory of preferential grain boundary oxidation in ZnO [79] and the concept/possibility of complexion (grain boundary phase-like) transitions [52]. Conducting flash sintering in a reduced atmosphere (Ar + 5% H_2) eliminated the asymmetrical grain growth (Fig. 5(b)), attesting the hypothesis that grain boundary oxidation transition is the root cause for anode-side abnormal grain growth [13].

AC flash sintering can eliminate the anode-cathode disparity in grain sizes. However, when the specimens are large, nonuniform temperatures can also result in grain size differences across the samples, which may be controlled under the guidance of multi-physics modeling.

There are also more conventional electric field/current effects in ZnO, including: (1) electric field induced migration of aliovalent cations (*e.g.*, $Al_{Zn}^{\bullet}$ in Al_2O_3-doped ZnO; unpublished results) and (2) growth of aligned ZnO single-crystalline rods along the electric field direction at a high current density [9]. Cathodoluminescence spectroscopy revealed excess amounts of point defects, formed inhomogeneously in clusters, in flash-sintered ZnO [80].

Overall, a diversifying spectrum of electric field/current/potential effects on sintering, grain growth, microstructure/defects development, and phase transformation have been observed. Unfortunately, no general trend can be identified at this time, and the behaviors appear to be materials specific. In-depth studies are needed to confirm many of the observations and further understand their underlying mechanisms (probably case by case).

5. Reducing the Onset Flash Temperature

Flash sintering at ultra-low furnace temperatures (or ideally starting at room temperature) can have significant technological advantages. In an earlier attempt to significantly reduce the flash temperature, a high electric field of 2250 V/cm was applied to 8YSZ to reduce the onset flash sintering temperature to ~390 °C, but the specimen could not be sintered to a high density [81].

According to the model presented in §2, we can reduce the onset flash sintering temperature *via* increasing the specimen conductivities. For example, we can substantially increase the conductivities of ZnO powder specimens *via* reducing the oxygen partial pressures in Ar + 5% H_2 to initiate a flash at a low furnace temperature of <120 °C; subsequently, ~97% of the theoretical density has been achieved (with uniform grain size of ~1 μm) in ~30 s [13]. Using ZnO as a model system, this study [13] discovered a strong dependence of flash sintering behaviors on the sintering atmosphere and pointed out a new direction to control flash sintering.

A most recent study further developed a water-assisted flash sintering (WAFS) technology. The conductivity of the ZnO powder specimen can be increased by >10,000 times *via* absorbing water vapor to enable a room-temperature flash; subsequently, the specimen can be densified to ~98% of the theoretical density in 30 s without any external furnace heating (Fig. 6). As a comparison, achieving similar densification *via* conventional sintering of ZnO (with a melting temperature of 1975 °C) typically requires firing at >1000 °C for hours. It is worth noting that Guillon and co-workers recently discovered that adding water in nanocrystalline ZnO can enhance densification in SPS/FAST [82,83]. However, it is yet unknown whether the water works only by increasing (surface) conductivity in the WAFS of ZnO, or whether it also

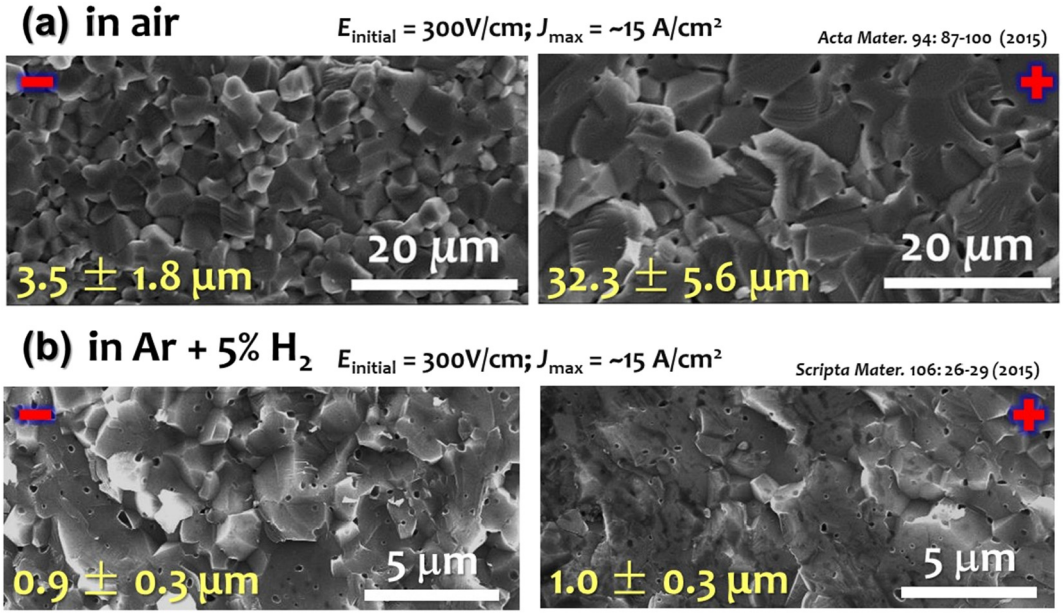

Fig. 5. Comparisons of the grain sizes at the anode and cathode sides of the specimens flash-sintered in (**a**) air and (**b**) Ar + 5% H_2. The anode-side abnormal grain growth was hypnotized to be resulted from an electric-potential-induced grain boundary oxidation (complexion) transition; this was evident for flash sintering with a large current density in air, but the anode-cathode grain-size disparity disappeared in the reduced atmosphere, attesting the above hypothesis. This figure is replotted after combining the results originally reported in refs. [9,13] with permission.

contributes to enhanced mass transport, similar to that in the cold sintering technology (CST) [84–86] or water-assisted SPS/FAST [82,83].

This new WAFS technology open yet another window for innovative ceramic fabrication with cost and energy savings, but extensive research and development must be done before it comes to commercial ceramic manufacturing.

Applied stresses can also reduce the flash temperature in flash-sinterforging [87], an effect that should be investigated, explored, and utilized in future studies.

6. Microstructure Control and Fabrication of Dense Nanocrystalline Ceramics

To date, virtually every flash sintering experiment starts with a constant-voltage (fixed initial field) mode that switches (shortly after the flash) to a current-controlled mode (that sets a maximum current or steady-state current density). This is neither the only, nor necessarily the optimal, route/method to conduct flash sintering experiments or subsequently large-scale fabrications.

To explore other flash sintering modes to control microstructural development, a new two-step flash sintering (TSFS) method has recently been developed to achieve fast densification with suppressed grain growth (Fig. 4) [12]. In TSFS, a specimen was first kept at a higher current of I_1 for a short duration t_1 after the onset of flash, and subsequently switched to a lower current of I_2 ($<I_1$) electronically for a longer duration t_2 ($>t_1$), as schematically illustrated in Fig. 4(b). Using ZnO as a model system, this TSFS method successfully achieved ~96.5% of the theoretical density with a grain size of ~370 nm, which represents a > 3 times reduction in final-stage grain growth in comparison with the conventional (one-step) flash sintering (Fig. 4(a)). Moreover, TSFS of ZnO achieved this result in a ~5 min, which is >200 times faster than the conventional two-step sintering of ZnO (that took ~15–20 h to achieve comparable results [88]). This cost-effective and energy-saving TSFS method can potentially be applied to other materials to achieve fast densification with suppressed grain growth (*e.g.*, eventually to fabricate dense nanocrystalline ceramics in minutes).

The recent work of TSFS of ZnO with a starting particle size of ~36 nm achieved a dense specimen of ~370 nm grain size (Fig. 4(a)) [12]. It may be possible to achieve nanocrystalline (with <100 nm grain sizes) dense specimens with TSFS with smaller starting particle sizes and further optimization of the processing parameters, but it has yet to be demonstrated.

The success of TSFS further suggests a new general direction to control the densification and microstructural evolution *via* manipulating

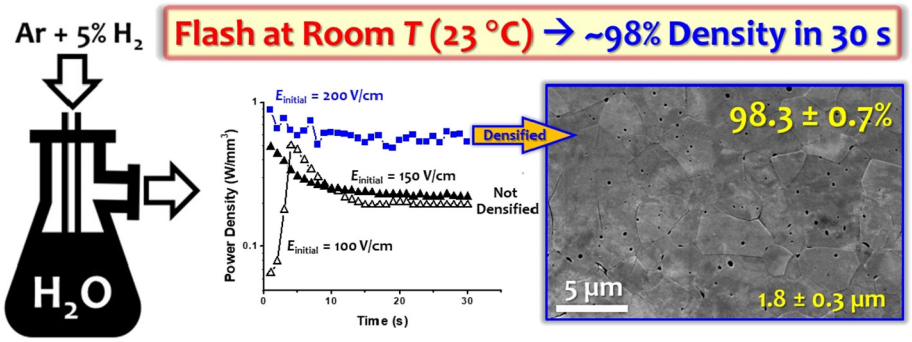

Fig. 6. Illustration of a new water-assisted flash sintering (WAFS) method: the adsorption of water vapor in a ZnO green specimen (of ~55% relative density) can promote the occurrence of a flash at room temperature and subsequently densify this ZnO specimen to ~98% relative density in 30 s. Reprint from ref. [10] with permission.

the $I(t)$ profile in flash sintering (to any pre-set profile) to achieve better or more customized results.

7. Selected Other Technological Developments and Issues

Researchers also reported similar flash sintering by using applied AC electric loadings, where the current flow though the specimens (instead of the electric field) is argued to be the key [89–91]. In fact, flash sintering of ionic conductors sometime requires AC loadings to allow reversible electrochemical reactions to sustain the currents to lead to substantial densifications [92].

Several "flash spark plasma sintering (FSPS)" methods for densifying more conductive ceramics (such as B_4C [93], *SiC* [94,95] and ZrB_2 [96]), as well as YSZ [97] and Nd-Fe-B based magnets [98], *via* forcing the occurrences of thermal runaways that do not occur naturally, have been developed.

Moreover, a contactless flash sintering method using plasma electrodes has been developed [99]. Most recently, a "flame-assisted flash sintering" has also been developed as a noncontact method to densify coatings on conductive substrates [100]. Yet another extension is represented by flash microwave sintering [101].

Most flash sintering experiments in laboratories have been conducted on small specimens (and the experiments on ZnO and 8YSZ reported here used 6 mm diameter pellets; see [8–13] for experimental details). Efforts have been made to scale up the flash sintering process. See two recent reviews [37,38] regarding the discussion about different specimen sizes and geometries, as well as the scaling-up efforts.

8. Summary and Outlook

It has been demonstrated that a flash starts as a coupled thermal and electric runaway in a variety of materials systems. A model has been developed to forecast the onset flash temperature *via* a graphical construction method. Two independent studies showed that ultrafast heating without applied electric field/current achieved similar densification and grain growth rates as the flash sintering with comparable heating profiles, suggesting that ultrahigh heating rates are the key for achieving rapid densification for at least ZnO and YSZ. Yet, studies discovered various electric field/current/potential effects on sintering, grain growth, microstructure and defects development, and phase transformation, most of which are likely materials specific and need further scrutiny. The onset flash sintering temperature can be reduced by several methods. Notably, a water-assisted flash sintering or WAFS method uses water to trigger a flash at room temperature to subsequently densify ZnO to ~98% densities in ~30 s. Another new two-step flash sintering or TSFS method enables the fabrication of dense ceramics with suppressed grain growth.

Several open scientific and technological questions are given and/or discussed as follows:

- Are there systems where the flashes are triggered by avalanches of non-equilibrium defects and/or first-order bulk phase (or interfacial phase-like) transformations with discontinuous increases in the specimen conductivities (so that the thermal runaway is a secondary process but not the primary cause)? What are their characteristic behaviors?
- The rapid densification mechanisms should be further investigated. Do non-equilibrium grain boundaries form in ultrafast heating and play a role in enhancing sintering rates? Are there some materials where the electric field/current enhanced densifications are significant or even dominant in flash sintering?
- In-depth studies should be conducted to confirm various electric field/current/potential effects on sintering, grain growth, microstructure and defects development, and phase transformation (with scrutiny), and further investigate their underlying mechanisms case by case. Are there any general trends or universal behaviors?
- Can WAFS and TSFS be applied to a broad range of other systems beyond ZnO?
- Can we control the densification and microstructural evolution *via* manipulating the $I(t)$ profile in the flash sintering (to any pre-set profile) to achieve better or more customized results beyond TSFS?

The author also believes that significant technological opportunities may exist in

- applying a pressure in flash sintering to further enhance densification and control microstructure development (beyond the flash-sinterforging experiment [87]);
- modifying flash sintering technologies to fabricate thin/thick films or membranes; and
- utilizing the contactless flash sintering technologies [99,100] to help fabricate ceramic coatings on metal/conductive substrates, *e.g.*, thermal/environmental barrier coatings.

Acknowledgement

This work is supported by the Aerospace Materials for Extreme Environments program of the U.S. Air Force Office of Scientific Research (AFOSR) under the grant no. FA9550-14-1-0174. We gratefully thank our AFOSR program manager, Dr. Ali Sayir, for his support and guidance. Jiuyuan Nie and Dr. Yuanyao Zhang are acknowledged for providing unpublished results in Figs. 2 and 3 and assistance in preparing figures.

References

[1] M. Cologna, B. Rashkova, R. Raj, J. Am. Ceram. Soc. 93 (2010) 3556–3559.
[2] R. Raj, M. Cologna, J.S.C. Francis, J. Am. Ceram. Soc. 94 (2011) 1941–1965.
[3] M. Cologna, A.L.G. Prette, R. Raj, J. Am. Ceram. Soc. 94 (2011) 316–319.
[4] Y.X. Du, A.J. Stevenson, D. Vernat, M. Diaz, D. Marinha, J. Eur. Ceram. Soc. 36 (2016) 749–759.
[5] J. Zhang, Z.H. Wang, T.Z. Jiang, L.Q. Xie, C. Sui, R.Z. Ren, J.S. Qiao, K.N. Sun, Ceram. Int. 43 (2017) 14037–14043.
[6] W. Ji, B. Parker, S. Falco, J.Y. Zhang, Z.Y. Fu, R.I. Todd, J. Eur. Ceram. Soc. 37 (2017) 2547–2551.
[7] S.K. Jha, R. Raj, J. Am. Ceram. Soc. 97 (2014) 527–534.
[8] Y. Zhang, J. Nie, J. Luo, J. Ceram. Soc. Jpn. 124 (2016) 296–300.
[9] Y. Zhang, J.-I. Jung, J. Luo, Acta Mater. 94 (2015) 87–100.
[10] J. Nie, Y. Zhang, J.M. Chan, R. Huang, J. Luo, Scr. Mater. 142 (2018) 79–82.
[11] Y. Zhang, J. Nie, J.M. Chan, J. Luo, Acta Mater. 125 (2017) 465–475.
[12] J. Nie, Y. Zhang, J.M. Chan, S. Jiang, R. Huang, J. Luo, Scr. Mater. 141 (2017) 6–9.
[13] Y. Zhang, J. Luo, Scr. Mater. 106 (2015) 26–29.
[14] C. Schmerbauch, J. Gonzalez-Julian, R. Roeder, C. Ronning, O. Guillon, J. Am. Ceram. Soc. 97 (2014) 1728–1735.
[15] L.M. Jesus, R.S. Silva, R. Raj, J.C. M'Peko, J. Alloys Compd. 682 (2016) 753–758.
[16] A.L.G. Prette, M. Cologna, V. Sglavo, R. Raj, J. Power Sources 196 (2011) 2061–2065.
[17] A. Gaur, V.M. Sglavo, J. Eur. Ceram. Soc. 34 (2014) 2391–2400.
[18] H. Yoshida, P. Biswas, R. Johnson, M.K. Mohan, J. Am. Ceram. Soc. 100 (2017) 554–562.
[19] A. Gaur, V.M. Sglavo, J. Mater. Sci. 49 (2014) 6321–6332.
[20] K.N. Sun, J. Zhang, T.Z. Jiang, J.S. Qiao, W. Sun, D. Rooney, Z.H. Wang, Electrochim. Acta 196 (2016) 487–495.
[21] A. Karakuscu, M. Cologna, D. Yarotski, J. Won, J.S.C. Francis, R. Raj, B.P. Uberuaga, J. Am. Ceram. Soc. 95 (2012) 2531–2536.
[22] K. Naik, S.K. Jha, R. Raj, Scr. Mater. 118 (2016) 1–4.
[23] I. Bajpai, Y.H. Han, J. Yun, J. Francis, S. Kim, R. Raj, Adv. Appl. Ceram. 115 (2016) 276–281.
[24] X. Hao, Y. Liu, Z. Wang, J. Qiao, K. Sun, J. Power Sources 210 (2012) 86–91.
[25] M. Biesuz, G. Dell'Agli, L. Spiridigliozzi, C. Ferone, V.M. Sglavo, Ceram. Int. 42 (2016) 11766–11771.
[26] H. Yoshida, Y. Sakka, T. Yamamoto, J.-M. Lebrun, R. Raj, J. Eur. Ceram. Soc. 34 (2014) 991–1000.
[27] H. Yoshida, K. Morita, B.-N. Kim, Y. Sakka, T. Yamamoto, Acta Mater. 106 (2016) 344–352.
[28] J.U. Valdebenito, A. Akbari-Fakhrabadi, M.R. Viswanathan, Mater. Lett. 209 (2017) 291–294.
[29] W. Straka, S. Amoah, J. Schwartz, MRS Commun. 7 (2017) 677–682.
[30] R. McKinnon, S. Grasso, A. Tudball, M.J. Reece, J. Eur. Ceram. Soc. 37 (2017) 2787–2794.
[31] R. Muccillo, E.N.S. Muccillo, J. Eur. Ceram. Soc. 34 (2014) 915–923.
[32] D. Liu, Y. Gao, J. Liu, F. Liu, K. Li, H. Su, Y. Wang, L. An, Scr. Mater. 114 (2016) 108–111.
[33] D.G. Liu, Y. Gao, J.L. Liu, F.Z. Liu, K. Li, H.J. Su, Y.G. Wang, L.A. An, Scr. Mater. 114 (2016) 108–111.
[34] D.G. Liu, Y. Gao, J.L. Liu, K. Li, F.Z. Liu, Y.G. Wang, L.A. An, J. Eur. Ceram. Soc. 36 (2016) 2051–2055.

[35] E. Zapata-Solvas, S. Bonilla, P.R. Wilshaw, R.I. Todd, J. Eur. Ceram. Soc. 33 (2013) 2811–2816.
[36] D. Kok, S.K. Jha, R. Raj, M.L. Mecartney, J. Am. Ceram. Soc. 100 (2017) 3262–3268.
[37] M. Yu, S. Grasso, R. McKinnon, T. Saunders, M.J. Reece, Adv. Appl. Ceram. 116 (2017) 24–60.
[38] C.E.J. Dancer, Mater. Res. Express 3 (2016) 102001.
[39] S.K. Jha, K. Terauds, J.M. Lebrun, R. Raj, J. Ceram. Soc. Jpn. 124 (2016) 283–288.
[40] K.S. Naik, V.M. Sglavo, R. Raj, J. Eur. Ceram. Soc. 34 (2014) 4063–4067.
[41] E. Bichaud, J.M. Chaix, C. Carry, M. Kleitz, M.C. Steil, J. Eur. Ceram. Soc. 35 (2015) 2587–2592.
[42] K. Terauds, J.-M. Lebrun, H.-H. Lee, T.-Y. Jeon, S.-H. Lee, J.H. Je, R. Raj, J. Eur. Ceram. Soc. 35 (2015) 3195–3199.
[43] R. Raj, J. Am. Ceram. Soc. 99 (2016) 3226–3232.
[44] R.I. Todd, E. Zapata-Solvas, R.S. Bonilla, T. Sneddon, P.R. Wilshaw, J. Eur. Ceram. Soc. 35 (2015) 1865–1877.
[45] Y. Dong, I.W. Chen, J. Am. Ceram. Soc. 98 (2015) 2333–2335.
[46] Y. Dong, I.W. Chen, J. Am. Ceram. Soc. 98 (2015) 3624–3627.
[47] M.D. McCluskey, S.J. Jokela, J. Appl. Phys. 106 (2009), 071101.
[48] J.G.P. da Silva, H.A. Al-Qureshi, F. Keil, R. Janssen, J. Eur. Ceram. Soc. 36 (2016) 1261–1267.
[49] M. Biesuz, V.M. Sglavo, J. Eur. Ceram. Soc. 36 (2016) 2535–2542.
[50] R. Raj, J. Eur. Ceram. Soc. 32 (2012) 2293–2301.
[51] M. Cologna, J.S.C. Francis, R. Raj, J. Eur. Ceram. Soc. 31 (2011) 2827–2837.
[52] P.R. Cantwell, M. Tang, S.J. Dillon, J. Luo, G.S. Rohrer, M.P. Harmer, Acta Mater. 62 (2014) 1–48.
[53] W.D. Kaplan, D. Chatain, P. Wynblatt, W.C. Carter, J. Mater. Sci. 48 (2013) 5681–5717.
[54] J. Luo, J. Am. Ceram. Soc. 95 (2012) 2358–2371.
[55] J. Luo, Crit. Rev. Solid State Mater. Sci. 32 (2007) 67–109.
[56] J. Zhang, F. Meng, R.I. Todd, Z. Fu, Scr. Mater. 62 (2010) 658–661.
[57] S.-W. Kim, S.-J.L. Kang, I.W. Chen, J. Am. Ceram. Soc. 96 (2013) 1398–1406.
[58] S.-W. Kim, S.-J.L. Kang, I.W. Chen, J. Am. Ceram. Soc. 96 (2013) 1090–1098.
[59] I.W. Chen, S.-W. Kim, J. Li, S.-J.L. Kang, F. Huang, Adv. Energy Mater. 2 (2012) 1383–1389.
[60] E.K. Akdogan, I. Savkliyildiz, H. Bicer, W. Paxton, F. Toksoy, Z. Zhong, T. Tsakalakos, J. Appl. Phys. 113 (2013).
[61] J.-M. Lebrun, T.G. Morrissey, J.S.C. Francis, K.C. Seymour, W.M. Kriven, R. Raj, J. Am. Ceram. Soc. 98 (2015) 1493–1497.
[62] S.K. Jha, J.M. Lebrun, R. Raj, J. Eur. Ceram. Soc. 36 (2016) 733–739.
[63] S.K. Jha, J.M. Lebrun, K.C. Seymour, W.M. Kriven, R. Raj, J. Eur. Ceram. Soc. 36 (2016) 257–261.
[64] C. McLaren, W. Heffner, R. Tessarollo, R. Raj, H. Jain, Appl. Phys. Lett. 107 (2015) 184101.
[65] J.H. Gao, Q. Li, Y.Y. Li, F.P. Zhuo, Q.F. Yan, W.W. Cao, X.Q. Xi, Y.L. Zhang, X.C. Chu, Appl. Phys. Lett. 107 (2015), 072909.
[66] H. Conrad, D. Yang, Mater. Sci. Eng. A 528 (2011) 8523–8529.
[67] D. Yang, H. Conrad, Mater. Sci. Eng. A 528 (2011) 1221–1225.
[68] J. Obare, W.D. Griffin, H. Conrad, J. Mater. Sci. 47 (2012) 5141–5147.
[69] H. Conrad, J. Am. Ceram. Soc. 94 (2011) 3641–3642.
[70] D. Yang, H. Conrad, Scr. Mater. 63 (2010) 328–331.
[71] S. Ghosh, A.H. Chokshi, P. Lee, R. Raj, J. Am. Ceram. Soc. 92 (2009) 1856–1859.
[72] S.W. Kim, S.G. Kim, J.I. Jung, S.J.L. Kang, I.W. Chen, J. Am. Ceram. Soc. 94 (2011) 4231–4238.
[73] Y. Dong, H. Wang, I.W. Chen, J. Am. Ceram. Soc. 100 (2017) 876–886.
[74] Y. Dong, I.W. Chen, J. Am. Ceram. Soc. (2017)https://doi.org/10.1111/jace.15274 (in press).
[75] W. Qin, H. Majidi, J. Yun, K. van Benthem, J. Am. Ceram. Soc. 99 (2016) 2253–2259.
[76] N. JomMorisaki, H. Yoshida, T. Tokunaga, K. Sasaki, T. Yamamoto, J. Am. Ceram. Soc. 100 (2017) 3851–3857.
[77] V. Tyrpekl, M. Naji, M. Holzhäuser, D. Freis, D. Prieur, P. Martin, B. Cremer, M. Murray-Farthing, M. Cologna, Sci. Rep. 7 (2017) 46625.
[78] W. Rheinheimer, M. Fülling, M.J. Hoffmann, J. Eur. Ceram. Soc. 36 (2016) 2773–2780.
[79] H.L. Tuller, J. Electroceram. 4 (1999) 33–40.
[80] H.T. Gao, T.J. Asel, J.W. Cox, Y.Y. Zhang, J. Luo, L.J. Brillson, J. Appl. Phys. 120 (2016) 105302.
[81] J.A. Downs, V.M. Sglavo, J. Am. Ceram. Soc. 96 (2013) 1342–1344.
[82] B. Dargatz, J. Gonzalez-Julian, M. Bram, P. Jakes, A. Besmehn, L. Schade, R. Roder, C. Ronning, O. Guillon, J. Eur. Ceram. Soc. 36 (2016) 1207–1220.
[83] B. Dargatz, J. Gonzalez-Julian, M. Bram, Y. Shinoda, F. Wakai, O. Guillon, J. Eur. Ceram. Soc. 36 (2016) 1221–1232.
[84] J. Guo, S.S. Berbano, H.Z. Guo, A.L. Baker, M.T. Lanagan, C.A. Randall, Adv. Funct. Mater. 26 (2016) 7115–7121.
[85] J. Guo, H.Z. Guo, A.L. Baker, M.T. Lanagan, E.R. Kupp, G.L. Messing, C.A. Randall, Angew. Chem. Int. Ed. 55 (2016) 11457–11461.
[86] J.-P. Maria, X. Kang, R.D. Floyd, E.C. Dickey, H. Guo, J. Guo, A. Baker, S. Funihashi, C.A. Randall, J. Mater. Res. 32 (2017) 3205–3218.
[87] J.S.C. Francis, R. Raj, J. Am. Ceram. Soc. 95 (2012) 138–146.
[88] M. Mazaheri, A.M. Zahedi, S.K. Sadrnezhaad, J. Am. Ceram. Soc. 91 (2008) 56–63.
[89] R. Muccillo, M. Kleitz, E.N.S. Muccillo, J. Eur. Ceram. Soc. 31 (2011) 1517–1521.
[90] R. Muccillo, E.N.S. Muccillo, M. Kleitz, J. Eur. Ceram. Soc. 32 (2012) 2311–2316.
[91] R. Baraki, S. Schwarz, O. Guillon, J. Am. Ceram. Soc. 95 (2012) 75–78.
[92] L.B. Caliman, R. Bouchet, D. Gouvea, P. Soudant, M.C. Steil, J. Eur. Ceram. Soc. 36 (2016) 1253–1260.
[93] B. Niu, F. Zhang, J. Zhang, W. Ji, W. Wang, Z. Fu, Scr. Mater. 116 (2016) 127–130.
[94] S. Grasso, T. Saunders, H. Porwal, B. Milsom, A. Tudball, M. Reece, J. Am. Ceram. Soc. 99 (2016) 1534–1543.
[95] E.A. Olevsky, S.M. Rolfing, A.L. Maximenko, Sci. Rep. 6 (2016) 33408.
[96] S. Grasso, T. Saunders, H. Porwal, O. Cedillos-Barraza, D.D. Jayaseelan, W.E. Lee, M.J. Reece, J. Am. Ceram. Soc. 97 (2014) 2405–2408.
[97] O. Vasylkiv, H. Borodianska, Y. Sakka, D. Demirskyi, Scr. Mater. 121 (2016) 32–36.
[98] E. Castle, S. Grasso, M. Reece, R. Sheridan, A. Walton, J. Magn. Magn. Mater. 417 (2016) 279–283.
[99] T. Saunders, S. Grasso, M.J. Reece, Sci. Rep. 6 (2016) 27277.
[100] S.L. Johnson, G. Venugopal, A.T. Hunt, J. Am. Ceram. Soc. 101 (2017) 536–541.
[101] Y.V. Bykov, S.V. Egorov, A.G. Eremeev, V.V. Kholoptsev, K.I. Rybakov, A.A. Sorokin, J. Am. Ceram. Soc. 98 (2015) 3518–3524.